Journal of Molecular Structure 1077 (2014) 101–113

Contents lists available at ScienceDirect

Journal of Molecular Structure

journal homepage: www.elsevier.com/locate/molstruc

MicroScale Thermophoresis: Interaction analysis and beyond ☆

Moran Jerabek-Willemsen [a], Timon André [a,b], Randy Wanner [a,c], Heide Marie Roth [a], Stefan Duhr [a], Philipp Baaske [a], Dennis Breitsprecher [a,*]

[a] Nanotemper Technologies GmbH, Flößergasse 4, 81369 Munich, Germany
[b] Heidelberg University, Biochemistry Center (BZH), Im Neuenheimer Feld 328, D-69120 Heidelberg, Germany
[c] Department of Pharmacy, Pharmaceutical Technology & Biopharmaceutics, Butenandtstr. 5, D-81377 Munich, Germany

HIGHLIGHTS

- MicroScale Thermophoresis (MST) measures dissociation constants down to 1 picomolar.
- MST can dissect different binding mechanism by distinct thermophoresis signals.
- MST quantifies dissociation constants in 100% cell lysate.
- MST can be used to determine thermodynamic parameters for interactions.
- MST can be used to monitor enzyme kinetics and protein folding.

GRAPHICAL ABSTRACT

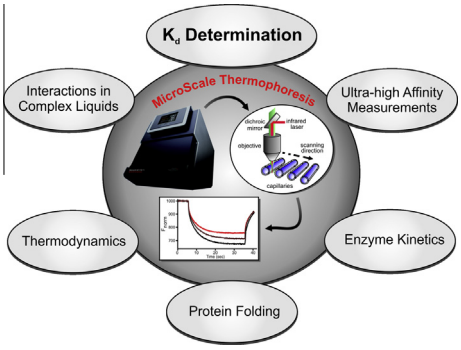

ARTICLE INFO

Article history:
Received 16 October 2013
Received in revised form 21 February 2014
Accepted 4 March 2014
Available online 16 March 2014

Keywords:
Microscale Thermophoresis
Interaction analysis
Protein folding
SPR
ITC
Binding studies

ABSTRACT

MicroScale Thermophoresis (MST) is a powerful technique to quantify biomolecular interactions. It is based on thermophoresis, the directed movement of molecules in a temperature gradient, which strongly depends on a variety of molecular properties such as size, charge, hydration shell or conformation. Thus, this technique is highly sensitive to virtually any change in molecular properties, allowing for a precise quantification of molecular events independent of the size or nature of the investigated specimen.

During a MST experiment, a temperature gradient is induced by an infrared laser. The directed movement of molecules through the temperature gradient is detected and quantified using either covalently attached or intrinsic fluorophores. By combining the precision of fluorescence detection with the variability and sensitivity of thermophoresis, MST provides a flexible, robust and fast way to dissect molecular interactions.

In this review, we present recent progress and developments in MST technology and focus on MST applications beyond standard biomolecular interaction studies. By using different model systems, we introduce alternative MST applications – such as determination of binding stoichiometries and binding modes, analysis of protein unfolding, thermodynamics and enzyme kinetics. In addition, wedemonstrate the capability of MST to quantify high-affinity interactions with dissociation constants (K_ds) in the low picomolar (pM) range as well as protein–protein interactions in pure mammalian cell lysates.

Introduction

Fluorescent molecules are used in life-sciences to trace and analyze molecular interactions. Fluorescence-based techniques have become invaluable for a quantitative understanding of biological

☆ This article is part of a special issue titled "Fluorescence studies of biomolecular association processes. Towards a detailed understanding of spectroscopic, thermodynamic and structural aspects".

* Corresponding author. Tel.: +49 89 4522895 44.
E-mail address: dennis.breitsprecher@nanotemper.de (D. Breitsprecher).

http://dx.doi.org/10.1016/j.molstruc.2014.03.009
0022-2860/

processes [26]. They not only allow for the visualization and localization of proteins in cells by a vast number of microscopic techniques, but they are also extensively used *in vitro* to determine biophysical parameters of molecular processes, ranging from equilibrium binding constants and enzyme kinetics to thermodynamics and mechanisms of protein folding. Over the last decades, a growing number of fluorescent *in vitro* techniques helped to understand many aspects of biomolecular function, which is owed to the versatility, specificity and sensitivity of fluorescence-based methods [25].

Detecting the fluorescence of biomolecules allows for an analysis of their interaction in a variety of ways: Depending on the properties of the investigated system, fluorescence quenching, fluorescence correlation spectroscopy [36], anisotropy or Foerster resonance energy transfer can be used to analyze equilibrium constants of a given interaction [38]. However, these techniques are only suited to analyze a rather small subset of interactions, since they crucially depend on parameters such as molecule size and size-change upon binding, and the relative position of fluorophores towards each other [38]. Moreover, they often require large sample volumes, complex experimental setups or intensive data analysis [47].

The phenomenon of thermophoresis was first described by Ludwig [34], and describes the directed motion of molecules through a temperature gradient. In recent years, MicroScale Thermophoresis (MST) emerged as a revolutionary method to monitor the directed movement of fluorescent molecules through microscopic temperature gradients in µl-volumes, allowing for the precise analysis of binding events in a few microliter solution of virtually any molecule – independent of size or physical properties [28,71,77]. MST circumvents the above mentioned limitations of other fluorescence-based methods by detecting changes in the hydration shell of biomolecules in addition to size-changes [19,21]. Therefore, MST can even detect events such as binding of small molecules to proteins, substrates to enzymes, or ligands to liposomes. Moreover, MST also offers advances over the most common non-fluorescent methods such as isothermal titration calorimetry (ITC) or surface plasmon resonance (SPR), by avoiding surface immobilization and high sample consumption. In addition, MST can be performed in virtually any buffer, even in plasma and cell lysate [54,71]. Recent technical advances now also allow for harnessing the intrinsic fluorescence of tryptophan-containing proteins to follow their thermophoresis, thereby providing a novel, entirely label-free and immobilization-free approach to study molecular interactions [55].

The biophysical background of MST was reported previously [20,21,28,54]. Thermophoresis describes a directed movement of particles in a temperature gradient. A temperature difference ΔT in space leads to a depletion of the solvated biomolecules in the region of elevated temperature, quantified by the Soret coefficient S_T: $c_{hot}/c_{cold} = \exp(-S_T \Delta T)$. This thermophoretic depletion depends on the interface between molecule and solvent. Under constant buffer conditions, thermophoresis probes the size, charge and solvation entropy of the molecules. The thermophoresis of a protein typically differs significantly from the thermophoresis of a protein–ligand complex due to binding-induced changes in size, charge and solvation energy. Even if a binding does not significantly change the size or charge of a protein, MicroScale Thermophoresis can still detect the binding due to binding-induced changes in the molecules solvation entropy [54].

The experimental setup for detecting MicroScale Thermophoresis is as follows: In devices of the Monolith-series (e.g. in the Monolith NT.115, Fig. 1A), thermophoresis is induced and detected in small glass capillaries which contain a solution of fluorescent molecules. An infrared (IR) laser with an emission wavelength of 1480 nm is focused through an objective into the capillary to produce a microscopic temperature gradient spanning 2–6 °C in a volume with a diameter of ~50 µm. While inducing the temperature gradient, the fluorophores in solution are excited and their emitted fluorescence is collected through the same objective as the infrared laser (Fig. 1B). This setup allows for following the thermophoresis dependent depletion (or accumulation) of fluorophores within the IR-laser-induced temperature gradient (Fig. 1C). For deriving binding constants, multiple capillaries with constant concentrations of fluorescent molecule and increasing concentrations of ligand are scanned consecutively and thermophoresis is detected (Fig. 1B and D). Changes in thermophoresis of the fluorescent molecules due to binding to ligand can then be used to calculate equilibrium binding constants (Fig. 1D). There are a number of different devices available to monitor MicroScale Thermophoresis: The Monolith NT.115/Monolith.NT115^{Pico} instruments as well as the Monolith NT.LabelFree, each with different detector types, allowing for the detection of tryptophan fluorescence as well as for the detection of visible light with wavelengths between 480 and 720 nm. The Monolith.NT115^{Pico} is designed to detect even low picomolar (pM) concentrations of red-emitting fluorophores to enable the analysis of high affinity interactions with dissociation constants (K_ds) in the low pM range. The Monolith NT.Automated combines two of the above mentioned detector types and has high-throughput capabilities specifically tailored to meet the requirements of high throughput screening approaches.

In recent years, MST was successfully employed to analyze a large variety of bio-molecular interactions, ranging from oligonucleotide-interactions [6,7,23,70], protein–DNA interactions [18,37,45,53,63,76] and protein–protein interactions [5,29,33,65,72,73] to protein–small molecule [24,27,44,55,59,71] and protein–liposome interactions [66,67].

Besides the well-established capability of MST to accurately monitor molecular interactions and to derive dissociation constants, thermophoresis can also be used to obtain a number of other parameters to characterize biomolecular properties and interactions.

In this review we demonstrate the versatility of MST and show that it can be used to investigate different aspects of biomolecular function: We show that due to recent improvements in detector sensitivity and experimental approaches, MST now allows for the detection of molecular interactions even at low pM concentrations, thereby enabling the rapid and fast analysis of high-affinity interactions with K_ds down to 1 pM. Moreover, we here show that MST is not only suited to detect binding events, but that it can also be used to analyze binding modes and stoichiometries, as well as protein folding and unfolding processes and thermodynamic parameters. In addition, we demonstrate that MST is also capable of monitoring and quantifying enzyme kinetics. Lastly, we present affinity measurements of fluorescently tagged proteins in pure cell lysate, which will have a great impact on both, basic biomedical research as well as on the development of better pharmaceuticals.

Precise detection of high-affinity interactions using MicroScale Thermophoresis

The rational optimization of molecular interactions is becoming increasingly important in modern drug discovery processes. Despite its importance, the precise determination of K_ds in the low nM or even pM range still remains an obstacle when using many established methods. So far, surface plasmon resonance has been most widely used to detect high-affinity interactions. However, immobilization of biomolecules, surface-dependent changes in binding kinetics and extremely slow off rates of most high-affinity interactions are well-known problems specifically linked to SPR, often leading to over-estimations of affinities [35,62]. On the other hand, ITC measurements generally depend on the overall amount

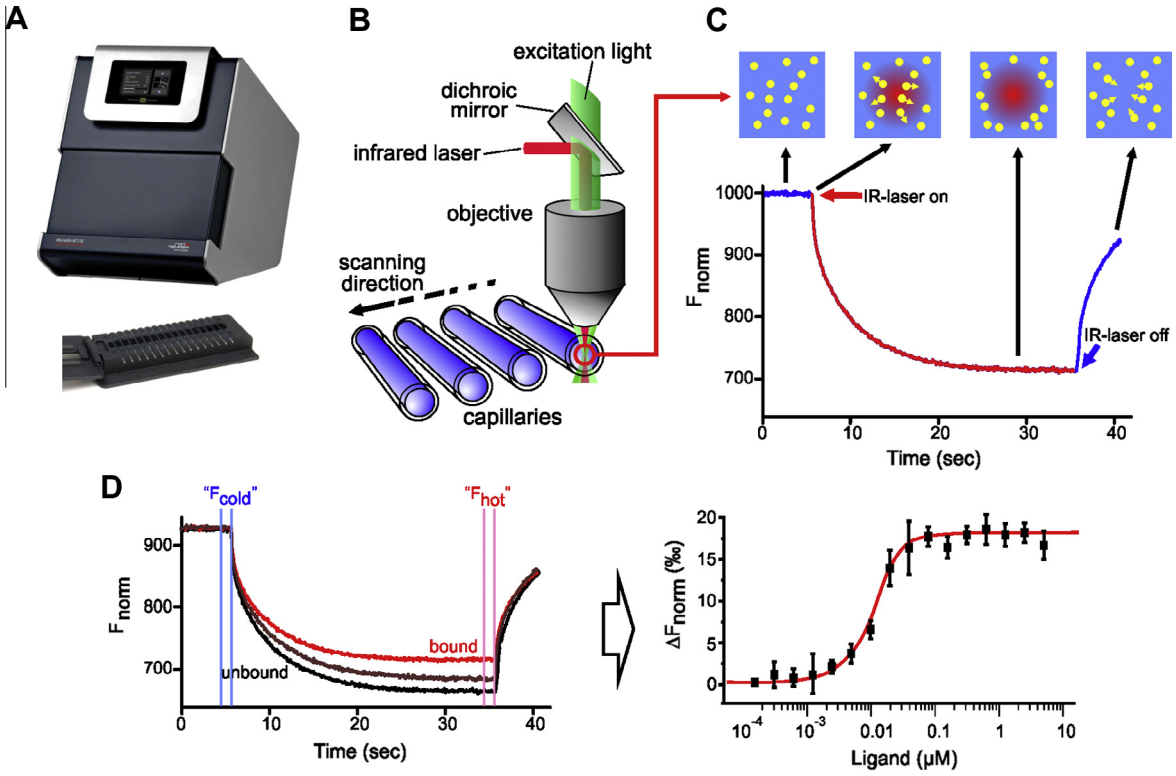

Fig. 1. MST setup and experiments. (A) The Monolith NT.115 from NanoTemper Technologies GmbH. The image below shows a capillary tray which can accommodate up to 16 capillaries. (B) Schematic representation of MST optics. MST is measured in capillaries with a total volume of ~4 μL. The fluorescence within the capillary is excited and detected through the same objective. A focused IR-Laser is used to locally heat a defined sample volume. Thermophoresis of fluorescent molecules through the temperature gradient is detected (C) Typical signal of a MST experiment. Initially, the molecules are homogeneously distributed and a constant "initial fluorescence" is detected. Within the first second after activation of the IR laser, the "T-Jump" is observed, which corresponds to a rapid change in fluorophore properties due to the fast temperature change. Subsequently, thermophoretic movement of the fluorescencently labeled molecules out of the heated sample volume can be detected. Typically, the fluorescence change is measured for 30 s. After deactivation of the IR-Laser, an inverse T-Jump occurs, followed by the "backdiffusion" of molecules, which is solely driven by mass diffusion. MST, Microscale Thermophoresis; IR, infrared; T-Jump, temperature jump. (D) Typical binding experiment. The thermophoretic movement of a fluorescent molecule (black trace; "unbound") changes upon binding to a non-fluorescent ligand (red trace; "bound"), resulting in different traces. For analysis, the change in thermophoresis is expressed as the change in the normalized fluoresence (ΔF_{norm}), which is defined as F_{hot}/F_{cold} (F-values correspond to average fluoresence values between defined areas marked by the red and blue cursors, respectively). Titration of the non-fluroescent ligand results in a gradual change in thermophoresis, which is plotted as ΔF_{norm} to yield a binding curve, which can be fitted to derive binding constants. (For interpretation of the references to color in this figure legend, the reader is referred to the web version of this article.)

of heat which is consumed/released by the binding event, limiting the biomolecule concentration for direct measurements to at least 10 nM, making it difficult to precisely detect K_ds in the low nM range.

One way to prevent surface-immobilization related problems and to boost assay sensitivity is to detect fluorescent molecules free in solution. Owed to ever improving fluorophore properties and detector sensitivity, the detection limit of fluorophores can be pushed to low pM concentrations. While more traditional approaches such as fluorescence correlation spectroscopy or fluorescence anisotropy measurements rely on large size-changes of the labeled molecule upon ligand binding and can require extensive and time-consuming assay optimization procedures, MST has the unique benefit of detecting even minute changes in the hydration shell of a molecule, thereby making it suitable for analyzing a variety of interactions independent of the nature and size of the molecule [28,71,77]. Moreover, the newly developed Monolith® NT.115^{Pico} device is capable of detecting fluorophores even at low pM concentrations in μl volumes, thereby combining an unmatched sensitivity for the analysis of high affinity interactions with minimal sample consumption.

Here we demonstrate that MST is a versatile method to detect interactions with K_ds in the pM range in entirely different experimental systems (Fig. 2). In a first set of experiments, we analyzed the hybridization reaction of 200 pM of a Cyanine5 (Cy5)-tagged oligo-nucleotide template with its complementary strand (Fig. 2A). Fitting of the relative change of thermophoresis upon DNA hybridization yielded a K_d of 167 ± 8 pM. This number is in good agreement with the K_d derived from theoretical calculations predicted from thermodynamic parameters (K_d = 180 pM, calculated with the IDT biophysics tool) [43], validating that MST can be used to derive exact binding affinities in the pM range for oligonucleotide-based reactions.

In another example, the binding of single-strand binding protein from *Escherichia coli* (EcoSSB) to a single stranded DNA (ssDNA) oligo(dT)$_{70}$ nucleotide was analyzed (Fig. 2B). EcoSSB plays a key role during DNA replication by binding ssDNA which is created by helicases, thereby preventing re-annealing of the strands and allowing replication by DNA primases and polymerases [3]. Biophysical *in vitro* and crystallographic studies showed that one EcoSSB tetramer binds a single ssDNA oligonucleotide over a length of 70 base-pairs [9,10,40]. The affinity of the interaction of EcoSSB and oligo(dT)$_{70}$ ssDNA is known be extremely high at physiological salt concentrations, with K_ds in the low pM or even fM range [10,16]. However, the exact affinity could not be determined yet due to the limited sensitivity of conventional methods. By using Cy5-labeled oligo(dT)$_{70}$ at a concentration of only 20 pM and titrating EcoSSB from 5 nM down to 10 fM, we could resolve a binding curve for the EcoSSB-oligo(dT)$_{70}$ interaction, yielding a K_d of 1 ± 0.1 pM. This demonstrates that MST allows for the precise analysis of high-affinity protein–DNA interactions that have been inaccessible up to now. MST is therefore a powerful tool

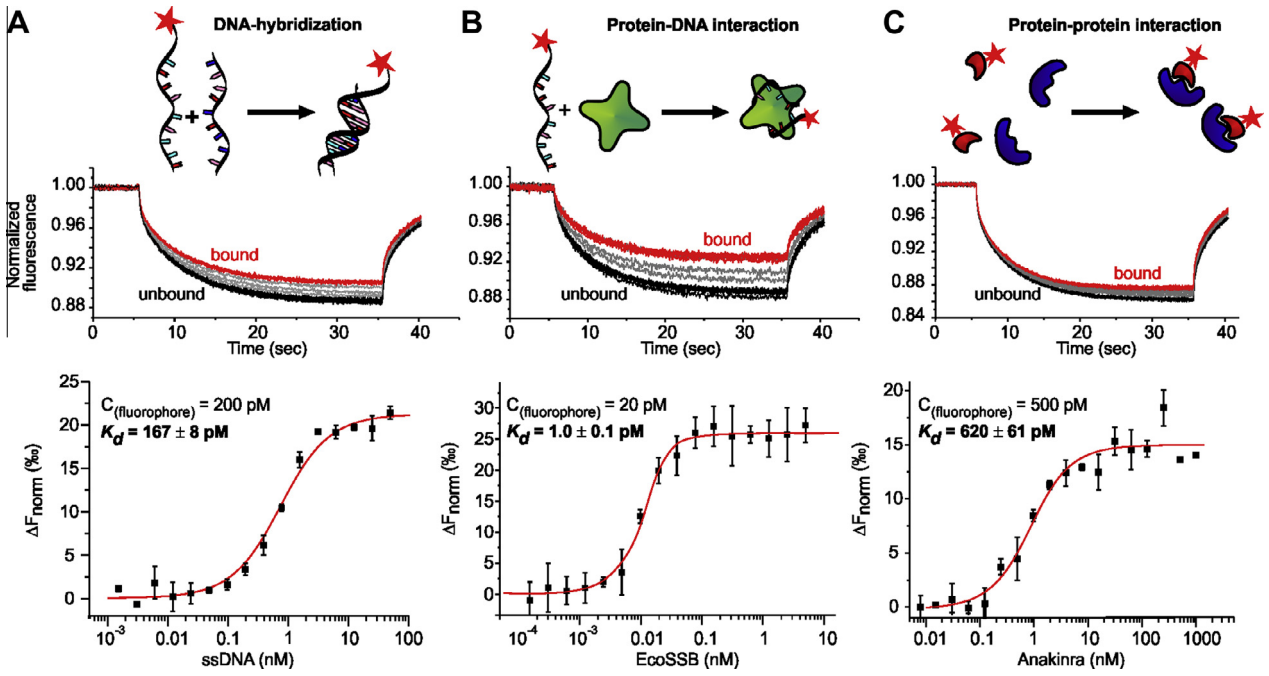

Fig. 2. Detection of picomolar K_ds of different experimental systems using the Monolith® NT.115^{Pico}. (A) DNA–DNA interaction. The hybridization of a 16mer with a complementary Cy5-labeled DNA strand was monitored with MST. Traces corresponding to the titration of complementary strand against 200 pM of Cy5-labeled template is shown. The change in MST signals was fitted (red line) to yield a K_d of 167 ± 8 pM. Error bars = s.d.; n = 3. (B) Protein–DNA interaction. Association of single strand binding protein from *E. coli* (EcoSSB) with a Cy5-labeled oligo-nucleotide $(dT)_{70}$ was monitored by titrating EcoSSB from 5 nM to ~100 fM against 20 pM Cy5-labeled DNA. Changes in thermophoresis were plotted, yielding a K_d of 1 ± 0.1 pM. Error bars = s.d.; n = 3. (C) Protein–protein interaction. Native Anakinra at concentrations from 1 μM down to 30 pM was titrated against 500 pM of NT647-labeled, soluble fragment of the Interleukin-1 receptor. Plotting of the change in thermophoresis and concomitant fitting of the data yielded a K_d of 620 ± 61 pM. Error bars = s.d.; n = 3.

to dissect virtually any molecular interaction involving DNA–protein crosstalk.

Finally, MST can also be used to detect and quantify high-affinity protein–protein interactions (Fig. 2C). Such interactions are of particular interest in biomedical research, as many therapeutic proteins are modified and optimized in order to treat diseases such as diverse cancer types or auto-immune disorders more efficiently [41,42]. A precise knowledge of the affinity of a therapeutic protein towards its target is essential for its optimization by rational design, as well as for testing if and how modifications of therapeutic proteins affect target binding [14,50]. One well known therapeutic protein is Anakinra, an interleukin-1 (IL-1) receptor antagonist [17,31,32]. It binds to the IL-1 receptor, thereby blocking the activity of IL-1 and as a consequence reducing symptoms of rheumatoid arthritis [15,52]. MST analysis using native Anakinra protein titrated against 500 pM of a NT-647 labeled, soluble fragment of the IL-1 receptor yielded a K_d of 620 ± 61 pM, rendering Anakinra a high-affinity binder. The obtained results are in good agreement with previously published values [58], and can be used to further deepen our understanding of this interaction. Moreover, MST can be used to rapidly test effects of covalent modifications of Anakinra – or other high-affinity therapeutic molecules – that are aimed to increase affinity or enhance stability.

Taken together, the examples shown in Fig. 2 highlight that MST is a versatile, fast and precise technique to derive pM dissociation constants from high-affinity biomolecular interactions in entirely different experimental systems.

Determination of binding states and stoichiometries by MicroScale Thermophoresis

MST not only allows for a precise determination of binding constants, but can also be used to derive additional information about the molecular mechanism of the investigated interaction. For instance, MST can be used to discriminate between different binding modes, and can also be used to determine interaction stoichiometries.

The thermophoresis signal that is detected by the NT.115 and NT.LabelFree devices contains multiple pieces of information: Upon activation of the IR-laser (which establishes the local temperature gradient) the temperature jump (T-jump) of the fluorophore is detected. It describes the rapid change in the photo physical properties of the fluorophore upon heating, and occurs within less than a second. Importantly, the T-jump predominantly depends on the local surroundings of the fluorophore and can thus be affected e.g. by binding of ligands in close vicinity. In contrast, thermophoresis depends globally on the properties of the entire molecule/complex, and is a comparably slow process that occurs on a second to minute time scale (Fig. 3A). In many cases, either the thermophoresis or T-Jump signal can be used to derive a dissociation constant. However, both signals also yield different information about the molecular interaction mechanism, which is owed to their different physical origin, and can thus be used independently to address different aspects of molecular interactions.

Here we demonstrate that T-jump and thermophoresis signals provide different mechanistic information about binding stoichiometries as well as binding modes by investigating binding of ssDNA to EcoSSB. As shown in Fig. 2B, EcoSSB binds to oligo$(dT)_{70}$ with very high affinity. Extensive biophysical characterization of this interaction has shown that EcoSSB and oligo$(dT)_{70}$ bind with a 1:1 stoichiometry. A shorter oligonucleotide, oligo$(dT)_{35}$, was shown to bind to EcoSSB with almost equally high affinity, but in a 2:1 stoichiometry [10].

The MST time traces of the titration of Cy5-labeled oligo$(dT)_{70}$ or oligo$(dT)_{35}$ with EcoSSB as well as the corresponding thermophoresis signals showed striking differences (Fig. 3A and B): While the titration curve of oligo$(dT)_{70}$ displays a typical, sigmoidal

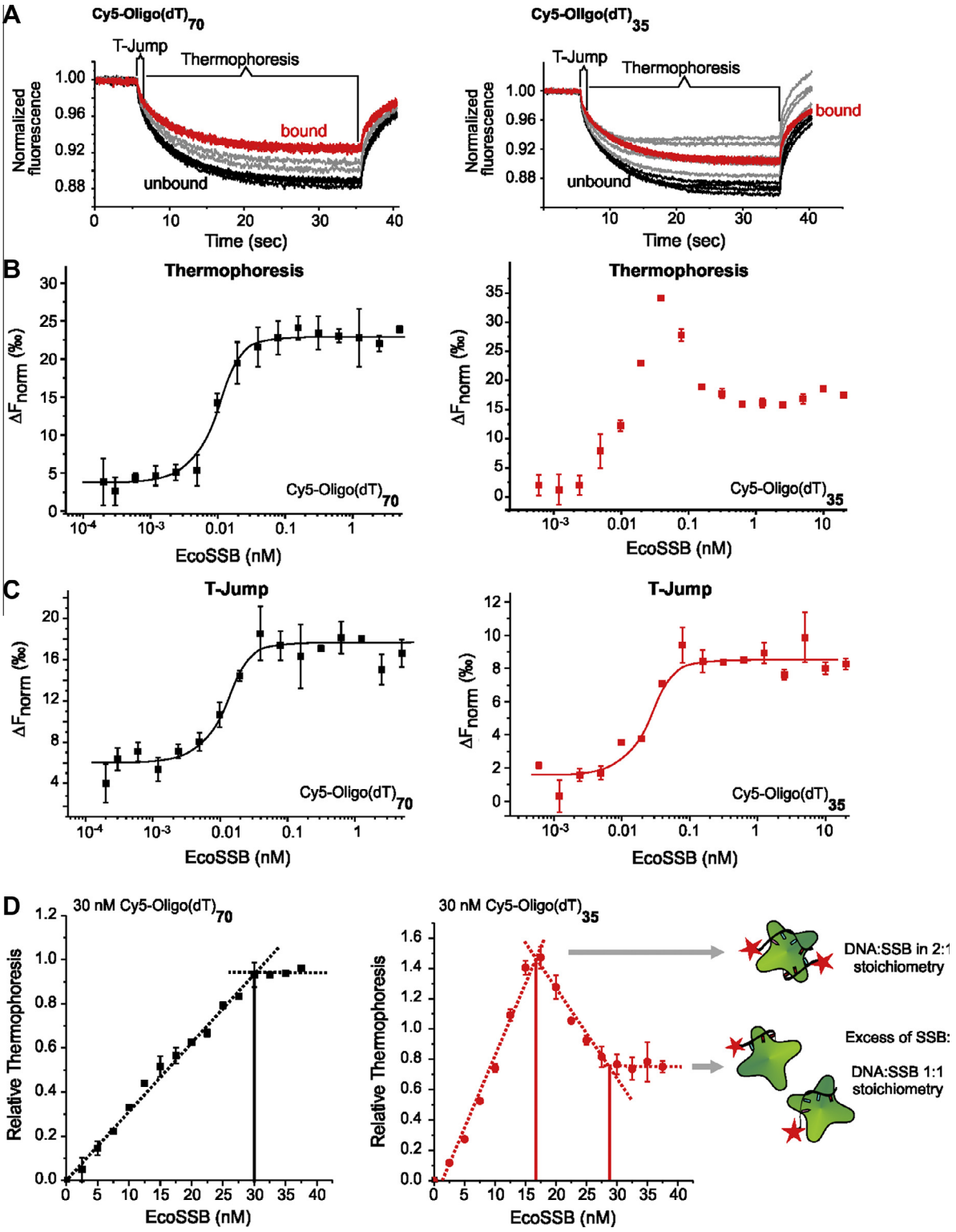

Fig. 3. MST of the interaction of EcoSSB with Cy5-$(dT)_{70}$ and Cy5-$(dT)_{35}$ ssDNA allows for determination of stoichiometries and binding modes. (A) Comparison of MST traces of titrations of EcoSSB against 20 pM Cy5-$(dT)_{70}$ (left) and 100 pM Cy5-$(dT)_{35}$ (right). Traces corresponding to bound and unbound states are colored black and red, respectively, traces corresponding to partially bound intermediates are shown in gray. Regions of the traces corresponding to T-Jump and thermophoresis signals are highlighted. (B) Thermophoresis signal from experiments equivalent to those shown in (A). Error bars = s.d.; $n = 3$. (C) T-Jump signal from experiments equivalent to those shown in (A). Error bars = s.d.; $n = 3$. (D) Thermophoresis signals of the titration of EcoSSB from 40 to 0 nM against 30 nM Cy5-oligo$(dT)_{70}$ (left) and Cy5-oligo$(dT)_{35}$ (right). Dotted lines represent linear extrapolations. Solid lines highlight "kinks" in those saturation curves, which correspond to different occupancies of EcoSSB with Cy5-oligo(dT) constructs. Error bars = s.d.; $n = 2$.

shape, the titration curve of oligo$(dT)_{35}$ displays an atypical peak in the thermophoresis signal close to the apparent point of saturation. Interestingly however, this peak is no longer observable when analyzing the T-jump signal (Fig. 3C), suggesting that the local changes that affect fluorescence upon binding of either oligo$(dT)_{70}$ or oligo$(dT)_{35}$ are identical, but that different molecular species

with different thermophoretic properties are formed by binding of EcoSSB to the different oligo-nucleotides.

To analyze the differences in the thermophoretic behavior of oligo(dT)$_{70}$ and oligo(dT)$_{35}$ and its dependence on EcoSSB in more detail, a saturation experiment was performed, in which a narrower range of EcoSSB (0–40 nM) was titrated against higher concentrations of Cy5-labeled oligonucleotides (30 nM). Under these conditions, added EcoSSB is completely bound to the oligonucleotide until saturation is reached, resulting in a linear increase of the MST signal. At EcoSSB concentrations at and above the saturation point, the thermophoresis signal does not change and remains constant despite further addition of EcoSSB. For the interaction of Cy5-oligo(dT)$_{70}$ with EcoSSB, a saturation curve was obtained with a clear saturation "kink" at 30 nM EcoSSB, validating the previously reported 1:1 stochiometry of this interaction. Interestingly, the same experiment with Cy5-oligo(dT)$_{35}$ yielded different thermophoresis signals. Here, the signal first increased with increasing EcoSSB concentrations and reached a peak at around 15 nM, but then decreased again to reach a second "kink" at around 30 nM EcoSSB. The positions of the different "kinks" in this case likely recapitulate EcoSSB concentrations at which different species of oligonucleotide-EcoSSB complexes are formed. At 15 nM EcoSSB, each EcoSSB molecule is saturated with two Cy5- oligo(dT)$_{35}$ molecules, resulting in a 2:1 stoichiometry [9,10] (Fig. 3D). Addition of EcoSSB at concentrations >15 nM results in a decrease of occupancy, until only one Cy5-oligo(dT)$_{35}$ molecule is bound per EcoSSB, which is reflected by the second kink around 30 nM (Fig. 3D). This effect is particularly pronounced since ssDNA fragments bind to EcoSSB with negative cooperativity (but high affinity), resulting in a homogenous mixture of oligo(dT)$_{35}$-EcoSSB 1:1 complexes. Importantly, the different species can only be identified by analyzing the thermophoresis signal, while the T-jump signal does not point towards two different species (compare Fig. 3B and C). The likely explanation for this is that the T-Jump signal solely depends on the local surrounding of the fluorophore, which should be independent of the occupancy of EcoSSB, while thermophoresis detects the different migration of the formed complexes in the temperature gradient, which is dictated by its size and hydration shell.

Thus, the presented example shows that MST signals contain binding information that exceed simple equilibrium constants, and that these information can be used to infer binding stoichiometries and binding modes for a given biomolecular interaction.

Using MicroScale Thermophoresis for thermodynamic analysis of biomolecular interactions

Biomolecular interactions display a remarkable degree of specificity, which is determined by distinct molecular recognition events. Binding between two interacting partners has enthalpic (ΔH°) and entropic ($T\Delta S^\circ$) components, corresponding to changes in both, structure and dynamics of each counterpart [8,51]. Both thermodynamic parameters are instrumental to elucidate the molecular mechanism of an interaction. Moreover, this knowledge can be used for the rational design of interactions, paving the way for novel pharmaceuticals or biomaterials [12] .

Importantly, thermodynamic parameters are not only accessible through the calorimetric measurement of reaction heat, but can also be extracted from the temperature dependence of the dissociation constant as shown by the following relations:

Given a reversible, bimolecular reaction

$$L + M \leftrightarrow LM$$

the dissociation constant K_d that is defined as

$$K_d = [\mathrm{L}]\frac{[\mathrm{M}]}{[\mathrm{LM}]} \quad (1)$$

which in turn directly depends on the Gibbs free energy change:

$$\Delta G^\circ = RT\ln(K_d) \quad (2)$$

Thus, by measuring K_ds over a temperature range, ΔG°, ΔH° and ΔS° can be calculated. Since MST is a powerful method to precisely determine K_ds with low sample consumption and on a short time scale, it is well suited for thermodynamic analyses of molecular interactions. The determination of thermodynamic parameters of a biomolecular interaction by MST is demonstrated in Fig. 4. In this example, we measured the DNA-hybridization equilibrium binding constant of a 16 base pair (bp) long oligo-nucleotide and a Cy5-labeled complementary template (Fig. 4A) over a range of temperatures using a Monolith NT115$^{\mathrm{Pico}}$ device. DNA hybridization can be readily detected by MST due to the different thermophoretic signals of ssDNA and dsDNA (Fig. 4B). At ambient temperatures, the K_d of the hybridization reaction was in the low nM to pM range (compare to Fig. 2A), but shifted towards significant higher values with increasing temperatures, as illustrated by the shift in the binding isotherms (Fig. 3C). K_d values for each temperature were calculated and plotted in a van't Hoff plot as $\ln(K_a)$ vs. $1/T$ (Fig. 4D). The temperature dependence of the association constant K_a (which equals $1/K_d$) was used to deduce the thermodynamic parameters ΔH and ΔS by linear extrapolation of the data in the van't Hoff plot. In addition, experiments were performed with two oligonucleotides carrying one or two mismatches, respectively (Fig. 4A). As expected, the hybridization affinity was greatly reduced for the mismatch-nucleotides, and the free enthalpy and entropy where higher compared to the perfect match hybridization reaction (Fig. 4D and E). One of the benefits of using DNA hybridization as a model system is that all interactions can be simulated in detail. We compared the experimentally determined thermodynamic parameters to calculated ones (using the IDT Biophysics tool http://biophysics.idtdna.com/) [43]. The comparison showed an excellent agreement of the parameters for the perfect match- as well as the mismatch hybridizations. We note that the parameters obtained for the mismatch construct with two mismatches shows the biggest divergence from the calculated parameters, which could however be due to limitations of the simulation software to correctly implement the effects of multiple mismatches rather than due to a larger experimental error.

Thus, MST-based K_d measurements at different temperatures can be used to derive thermodynamic parameters for biomolecular interactions, which can in turn be used to gain additional mechanistic information about the investigated system.

Monitoring thermophoretic shifts to dissect equilibrium protein unfolding

Thermophoresis can not only be used to dissect molecular interactions, but can also provide valuable information on the folding properties of proteins. Chemical denaturation of proteins is widely used to assess their stability and folding properties. Such analyses are particularly important for the design and optimization of therapeutic biomolecules, and are also necessary to understand in detail protein-misfolding related diseases [1,48].

It has recently been demonstrated that MST is well suited to follow protein unfolding and to detect unfolding intermediates, and that it rivals more traditional approaches such as circular dichroism or tryptophan fluorescence measurements in this capacity due to its speed and low sample consumption [4]. Here, we expand MST-based protein unfolding analyses using two well characterized model systems, bovine carbonic anhydrase II (BCAII) and concanavalin A (ConA). By using the NT.LableFree device, we show that

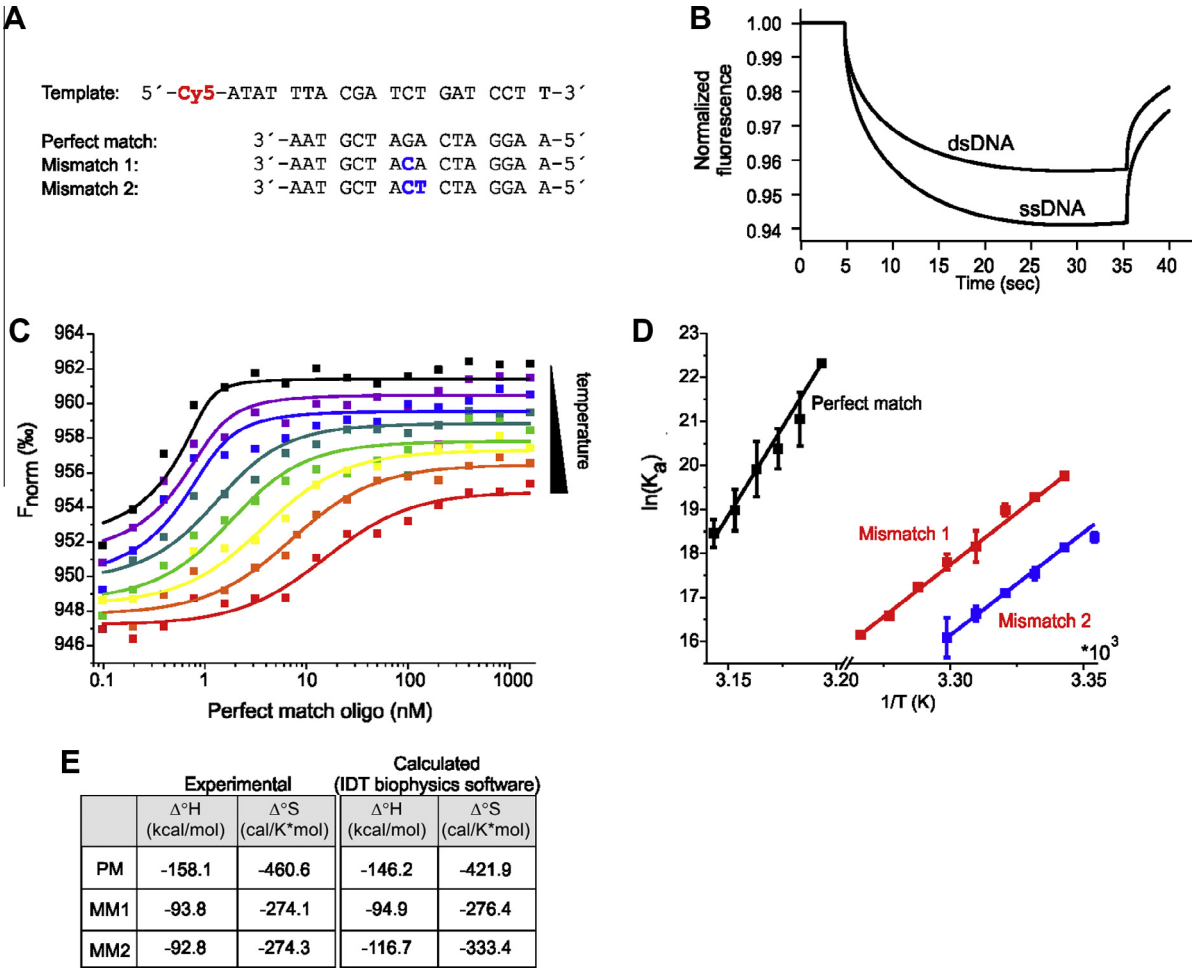

E

	Experimental		Calculated (IDT biophysics software)	
	Δ°H (kcal/mol)	Δ°S (cal/K*mol)	Δ°H (kcal/mol)	Δ°S (cal/K*mol)
PM	-158.1	-460.6	-146.2	-421.9
MM1	-93.8	-274.1	-94.9	-276.4
MM2	-92.8	-274.3	-116.7	-333.4

Fig. 4. Determination of thermodynamic parameters of DNA hybridization by MST. (A) Sequences of the DNA oligomers. Single base substitutions of the mismatches are highlighted in blue, 5′-terminal Cy5 in red. (B) Exemplary MST timetraces for a single-stranded (ssDNA) and a double-stranded DNA (dsDNA). ssDNA shows a stronger MST response then dsDNA. (C) Temperature-jump binding curves over a temperature range from 38 °C to 45 °C; increments 1 °C. (D) Van't Hoff plots of the DNA–DNA hybridization reactions. The template-PM, template-MM1 and template-MM2 interactions are shown in black, red and blue, respectively, Error bars = s.d.; $n = 2$; PM = perfect match, MM = mismatch. (E) Comparison between experimentally determined and calculated $\Delta H°$ and $\Delta S°$ values. (For interpretation of the references to color in this figure legend, the reader is referred to the web version of this article.)

MST can be used to monitor and characterize even complex chemical protein unfolding processes of untagged proteins in solution, and that it is even capable of detecting different unfolding intermediates such as molten globules.

The enzyme BCAII is of great pharmaceutical interest, since it is a drug target for compounds such as acetazolamid, methazolamide and dorzolamide which are used for the treatment of glaucoma [39]. BCAII is a globular, single domain protein which primarily contains beta-structures [22]. Its unfolding and folding behavior has been studied extensively using guanidine hydrochloride (GdmCl), revealing a complex unfolding process with several intermediate states [49,64,74]. Here we tested whether the BCAII unfolding mechanism that was previously characterized by combination of different methods can be reproduced by MST.

As shown in Fig. 5A, the thermophoresis signal of BCAII changes with increasing GdmCl concentrations. The MST results in Fig. 5A are directly compared to previously reported results in Fig. 4B and C [11], which were obtained either by measuring shifts in the intrinsic tryptophan fluorescence (Fig. 5B), or by measuring the fluorescence of the fluorophore 8-anilino-naphthalene-1-sulfonic acid (ANS) which non-specifically binds to the surface of proteins and serves as a reporter for unfolding processes (Fig. 5C). The thermophoresis of BCAII shows an initial, steep change already at GdmCl concentrations between 0 and 0.1 M. interestingly, a similar initial change can also be observed in the tryptophan fluorescence (Fig. 5B), but not in ANS fluorescence (Fig. 5C). A peak in thermophoresis can be observed between 1.2 and 1.5 M GdmCl, which correlates with a peak in ANS fluorescence (Fig. 5C). Enhanced ANS fluorescence is frequently used to identify partially folded intermediates – so-called molten globules – and likely stems from exposure of hydrophobic clusters at the protein surface [56,57]. The peak in ANS fluorescence during BCAII denaturation was interpreted to resemble such a stable molten globule intermediate [11]. However, ANS fluorescence analysis faces important drawbacks, since ANS binding to proteins might change protein folding and stability. Thus, based on our interpretation of the data that the MST peak in Fig. 5A represents the molten globule state, we propose that MST is especially well suited to detect such intermediates. This is due to the large changes in the hydration shell of the protein upon the exposure of hydrophobic patches on the protein surface, which is in line with previous studies [4]. Because detection of thermophoresis occurs via intrinsic tryptophan fluorescence, protein stability is not affected as it is by external reporter molecules such as ANS.

In a second example, we investigated the GdmCl-dependent changes in thermophoresis of ConA. ConA belongs to a protein

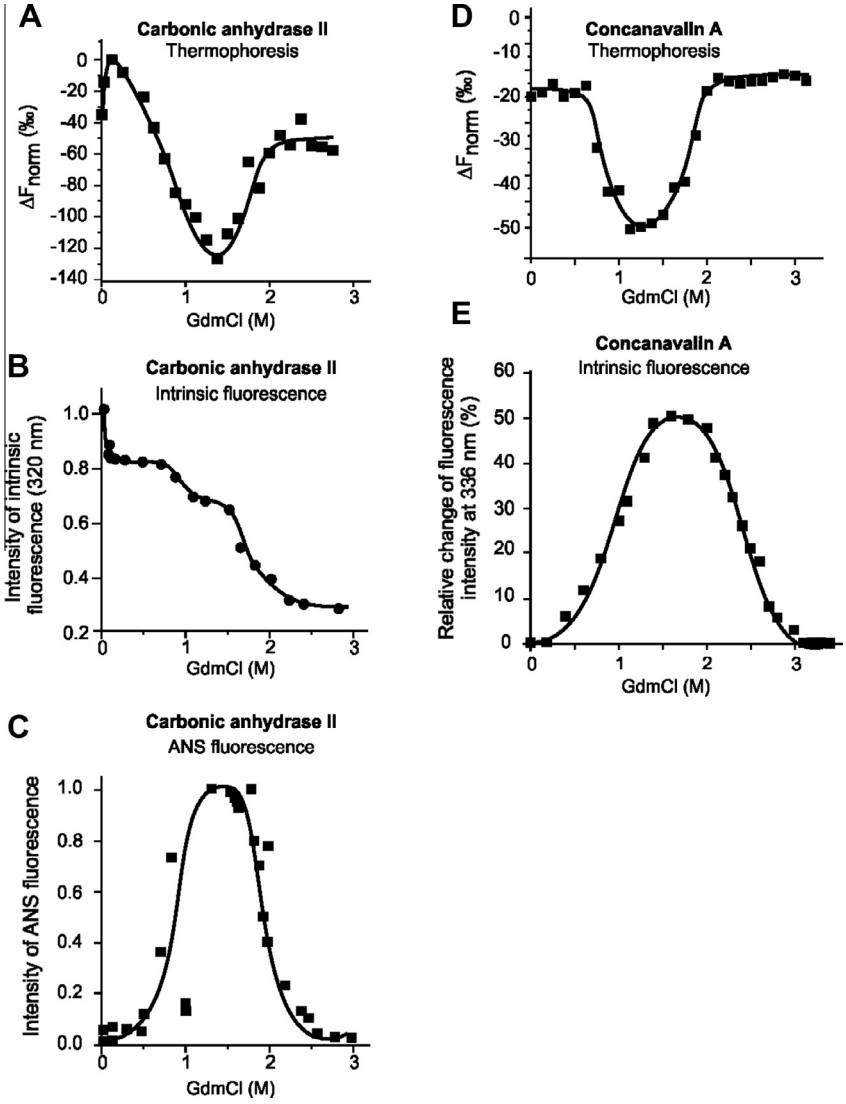

Fig. 5. Chemical equilibrium unfolding of BCAII and ConA analyzed by MST. (A) Change of thermophoresis of 1 μM BCAII monitored by detection of the intrinsic tryptophan fluorescence in the Monolith® NT.LabelFree instrument at GdmCl-concentrations from 0 to 3 M. (B and C) Data adopted from [11] are shown as a comparison. (D) Change in thermophoresis of 2 μM ConA monitored by detection of the intrinsic tryptophan fluorescence in the monolith NT.LabelFree at GdmCl-concentrations between 0 and 3 M. (E) Data adopted from [13] are shown as a comparison.

family referred to as lectins, which are used in numerous biological applications. For instance, they are used to probe normal or cancer cells, to study glycosylation states of cells and also in labs to prepare polysaccharides and glycopeptides using affinity chromatography [60,61]. Previously it was shown by chemical denaturation that ConA unfolding follows a three-step mechanism. As shown in Fig. 4D, the GdmCl-induced unfolding of ConA results in a characteristic thermophoresis signal with two distinct transition states around 0.8 and 1.8 M GdmCl. At concentrations between 1 and 1.6 M GdmCl, an apparently stable intermediate is formed with significantly higher thermophoresis than the folded and completely unfolded ConA molecule (Fig. 5D). Equivalent transition states and a stable intermediate have been reported previously by detecting the relative change in tryptophan emission at 336 nm (Fig. 5E, [13]), again demonstrating that MST can recapitulate complex unfolding mechanisms of proteins. Given the low sample consumption and short measurement times, MST therefore constitutes an attractive alternative to analyze denaturant-induced equilibrium denaturation processes even of complex, multi-state unfolding reactions.

Analysis of enzyme kinetics by MicroScale Thermophoresis

In biomedical research, scientists do not only investigate equilibrium events, but also analyze enzyme kinetics to elucidate biochemical pathways, which is eventually important to understand if and how certain therapeutic compounds or biomolecules affect the underlying mechanisms inside the cell.

Here we show that MST can be used to analyze enzyme kinetics, using two different experimental approaches to follow the DNase I-mediated degradation of dsDNA. DNase I is a robust enzyme with Mg^{2+}-dependent endonuclease activity, which non-specifically cleaves DNA to release di-, tri- and oligonucleotide fragments with 5′-phosphorylated and 3′-hydroxylated ends (Fig. 6A) [30,68,69]. DNase I acts on single- and double-stranded DNA, as well as on chromatin and RNA:DNA hybrids. Owing to these characteristics, this enzyme is often used as a tool in molecular biology and is thus well characterized.

To investigate the nuclease activity of DNase I, we chose two different approaches: in a first approach nuclease activity was measured directly in time intervals of 3 s by repeatedly scanning

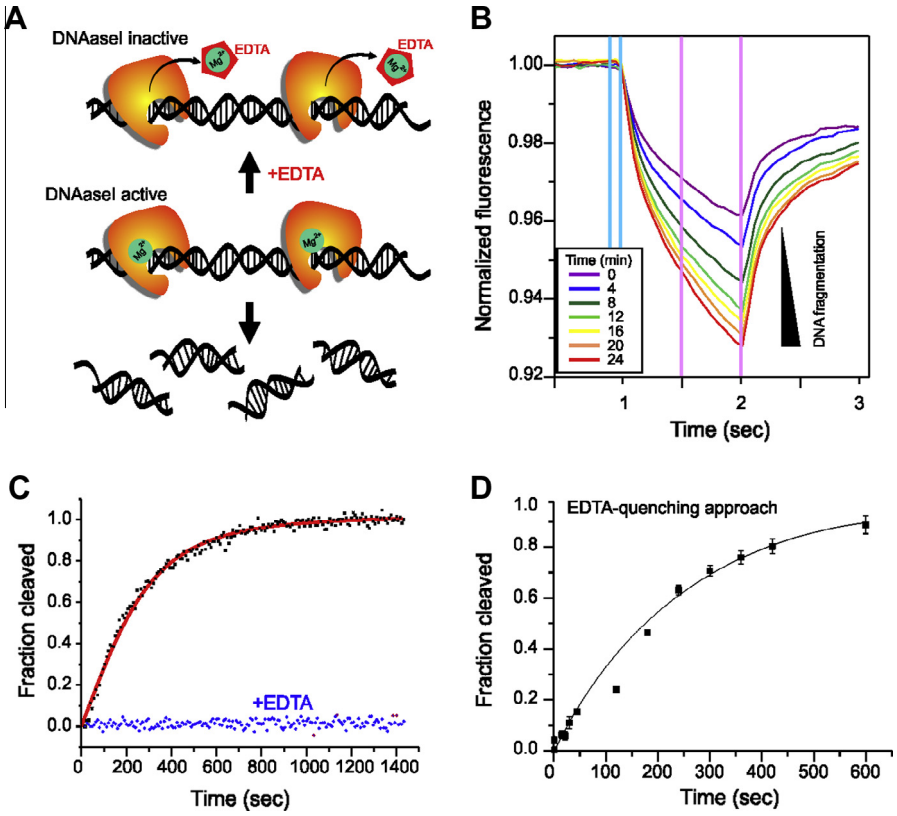

Fig. 6. Kinetics of the enzymatic degradation of DNA by DNase I using different MST-based approaches. (A) Schematic representation of the Mg^{2+}-dependent degradation of DNA by DNase I. (B) Real-time measurement of DNA degradation. Representative MST traces of the time-dependent degradation of SybrGold-labeled 110 bp dsDNA by DNase I are shown. DNA-thermophoresis increases with time, indicating fragmentation of the DNA. Blue and red lines represent boarders used for analyzing changes in thermophoresis. (C) Plot of the fraction of cleaved DNA determined from the thermophoresis signal over time from experiments in presence (blue) and absence (black) of 5 mM EDTA. The fit (red curve) yields a time constant of $\tau = 247$ s. (D) Quenching approach to monitor time-dependent DNA fragmentation by DNase I. The DNase I reaction was stopped after different incubation times by transferring the solution into EDTA-containing buffer. The samples were the analyzed by MST and the fraction of cleaved DNA was plotted against time. Error bars = s.d., $n = 2$. (For interpretation of the references to color in this figure legend, the reader is referred to the web version of this article.)

the same capillary and monitoring the thermophoresis-change of the SybrGold-labeled DNA substrate upon fragmentation (Fig. 6B). MST measurements were limited to short time spans in order to maximize the temporal resolution of the experiment. For these direct measurements, two experiments where performed. The buffer of the first reaction contained Mg^{2+} ions, DNase I and the DNA substrate, the second one additionally contained EDTA to inactivate DNase I by chelating Mg^{2+}, and thus served as a negative control to exclude effects such as photobleaching or spontaneous DNA degradation.

Both capillaries were scanned and MST measurements were performed in an alternating manner. The measurement times for each capillary were short, with each capillary measured for only 3 s:1 s laser off, 1 s laser on, 1 s laser off (Fig. 6B). Because of the alternating measurement of both capillaries, this time frame was in total 8 s for each capillary. MST experiments showed that thermophoresis of the DNA substrate changed significantly over time (Fig. 6B). In presence of EDTA however, the thermophoresis signal remains constant during the time course of the experiment, showing that changes in thermophoresis depend on DNase I activity and therefore reflect fragmentation of DNA into smaller pieces. Plotting the degree of fragmentation against time showed a typical hyperbolic shape which could be fitted to yield a time constant of $\tau = 247$ s (Fig. 6C).

In a second approach, the reaction was quenched chemically after 16 different incubation periods by transferring the reaction mixture into buffer containing EDTA. The samples were then loaded into capillaries and subjected to MST measurements. Changes in thermophoresis in dependence of incubation times before quenching were analyzed (Fig. 6D). This approach yielded similar results ($\tau = 260$ s) compared to the direct approach. Thus, by analyzing the changes in thermophoresis, we could determine DNase I enzyme kinetics, using both the direct measurement and the "quenched activity" approach. Importantly, by using a quenching approach reaction times can be chosen independently of the Monolith instrument settings, and can therefore be much less than 3 s (even with ms time resolution if using rapid-mixing devices for sample preparation). This example shows that MST can also be used to determine kinetic parameters of enzymes and other catalytic biomolecules.

Analysis of protein–protein interactions in pure cell lysate

The formation of protein–protein complexes plays an essential role in many biological processes. Intra- and extra-cellular signaling greatly depends on precisely coordinated interactions of proteins with other biomolecules. Traditionally, determination of binding affinities between biomolecules has been performed in highly diluted homogenous solutions, which are biochemically very different from the crowded mixtures of molecules inside the cell. Typically protein concentrations in binding assays are so low that they do not affect the physical properties of the solution. However the cellular environment contains high concentrations of many different biomolecules such as proteins, lipids, small molecules and nucleic acids, all of which together increase the viscosity

of the solution and therefore alter the diffusion of biomolecules. The biomolecules in those dense solutions bind to each other and also affect the molecules of interest via electrostatic, hydrophobic and van der Waals interactions, as well as by non-specific or specific steric interactions. Therefore it is important to have a better understanding how molecules interact with each other in highly crowded biomolecular environments [46]. Notably, however, the most common techniques, such as SPR and ITC, cannot be employed to study interactions in complex bioliquids.

Most of the crowding studies are generally performed *in vitro*, since the analysis of binding affinities in cells is very challenging. Typically, high concentrations of purified proteins or polymers like dextran, Ficoll and PEG are added as crowding agents to simple buffer solutions such as PBS, HEPES or TRIS to mimic cellular crowding. The binding experiments are then performed with and without crowding agents and the effects of a highly crowded environment can be studied [75].

Performing experiments with crowded solutions imposes different technical difficulties, primarily due to high viscosity and an increasing background signal. In addition, in many systems crowding reagents cannot reflect the much more complex environment in cells. Thus, for a truly quantitative understanding of molecular interactions, binding experiments have to be performed under *in vivo* like conditions (e.g. in eukaryotic cell lysate, plasma, or serum).

Such binding experiments are best performed using fluorescence fusion proteins such as GFP or mCherry due to the following advantages:

(1) Analysis of K_d values is possible without any protein-purification step. Many proteins lose activity upon protein purification.
(2) K_ds can be determined in highly crowded protein environment.
(3) Chemical labeling with fluorophores is not required.
(4) Access to thermodynamic parameters under *in vivo*-like conditions is possible (cell lysate, serum).

MST permits a robust and fast analysis of protein–protein interactions even in highly complex biological liquids. Here we have investigated the binding of TEM1 β-Lactamase to BLIP (β-Lactamase Inhibitory Protein) using MST.

In the first experiment, we investigated the binding of NT647-labeled TEM1 (covalently labeled on lysine residues) to BLIP. The concentration of NT647-labeled TEM1 was kept constant at 5 nM, while the concentration of BLIP was varied. The calculated K_d for the interaction between NT647-labeled TEM1 and BLIP was 4.2 nM ± 0.8 nM (Fig. 7A). The determined binding affinity correlates nicely with previously published data using MST and SPR [2,54].

In a second set of experiments we have studied the binding affinity of purified Ypet-BLIP to purified mCherry-TEM1. The concentration of Ypet-BLIP was kept constant at 10 nM, while the concentration of mChery-TEM1 was varied. The calculated K_d for the interaction between Ypet-BLIP and mChery-TEM1 was 17.7 nM ± 4 nM. (Fig. 7B), showing that the protein tags only minimally affect binding affinity. This result demonstrates that fluorescence fusion proteins are well suited to determine binding affinities by MST.

In a last set of experiments we have studied the binding affinity of Ypet-BLIP to mCherry-TEM1 in 100% highly crowded cell lysate from 293T cells. Ypet-BLIP was diluted in cell lysate to a final concentration of 10 nM and mixed with a mCherry-TEM1 dilution series in the same 293T cell lysate. The calculated K_d for the interaction between Ypet-BLIP and mChery-TEM1 was 13.8 nM ± 3.6 nM (Fig. 7C), recapitulating the affinity determined with the equivalent proteins in aqueous buffer.

These results underline the unique applicability of MicroScale Thermophoresis in studying biomolecular interactions directly in highly crowded cell lysates using fluorescence fusion proteins. In

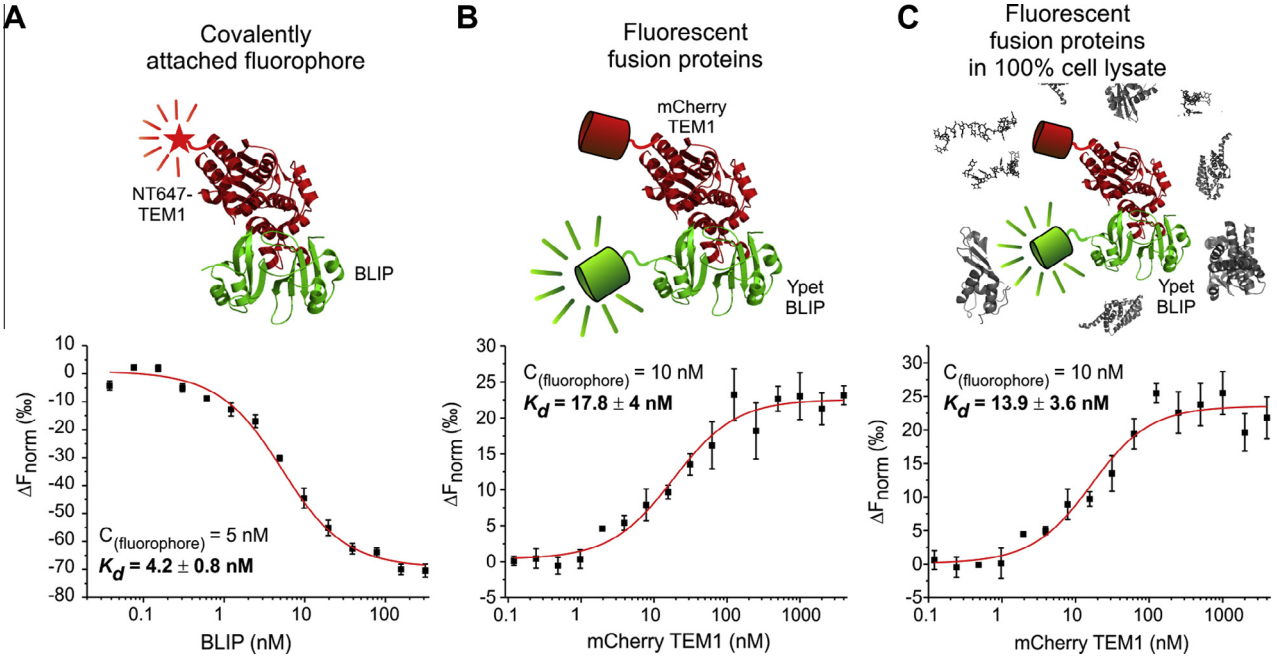

Fig. 7. Thermophoretic analysis of protein–protein interactions in pure cell lysate. (A) Interaction between NT647-labeled, purified TEM1 with purified BLIP. Changes in thermophoresis of a titration of BLIP at concentrations from 300 nM to 50 pM against 5 nM NT647-TEM are shown. The fit yielded a K_d of 4.2 ± 0.8 nM. Error bars = s.d., n = 2. (B) Interaction of purified mCherry-TEM1 with Ypet-BLIP in MST-buffer. Fit of the changes in thermophoresis signal yielded a K_d of 17.8 ± 4 nM. Error bars = s.d., n = 2. (C) Analysis of the same interaction as shown in (B) in 100% cell lysate instead of MST-buffer. Fit of the changes in thermophoresis signal yielded a K_d of 13.9 ± 3.6 nM. Error bars = s.d., n = 2.

principle, no protein purification is required in order to analyze protein–protein interactions under these conditions. The MST experiment can be performed with two different cell lysates expressing different fluorescence fusion proteins (fluorescence excitation of both fluorescence proteins should be different in order to avoid fluorescence artifacts). The concentration of the first binding partner is kept constant at low nM concentrations, while the concentration of the second binding partner is varied. The protein concentration can be easily estimated by preparing calibration curves using purified fluorescence proteins as Ypet/GFP/mCherry or by quantitative western blotting. On the basis of such a purification-free approach, a number of applications become possible. FRET signals for the protein–protein interaction in cells could be analyzed for instance, then the two lysates could be used for MST analysis, each of which is immuno-depleted for one of the proteins. This way, a comprehensive and quantitative characterization of protein–protein interactions on the cellular and molecular level would be accessible within a short amount of time. Even without knowing cellular concentrations of the expressed proteins, cell lysate approaches can be used to quickly verify if and how the proteins of interest interact under close-to-native conditions.

Concluding remarks

In this review, we give a comprehensive overview over Micro-Scale Thermophoresis applications that exceed the determination of equilibrium constants. We show that MST can be used to determine affinities of so far inaccessibly strong interactions with K_ds in the low pM range. Moreover, we demonstrate that thermophoresis signals of interacting proteins provide additional information about binding stoichiometries, binding modes and conformations. Remarkably, thermophoresis and T-jump signals can yield complementary information which can be used to quickly determine molecular mechanisms of biomolecular interactions. Lastly, the fluorescence-based approach of MST also allows for the quantification of K_ds even in 100% cell lysate, thereby paving the way for a quantitative understanding of interaction in a close-to-native context, which allows for testing drugs or therapeutic molecules directly in their target environment. Thus, for interaction analyses in complex bioliquids, MST offers huge advantages over other common approaches.

In addition to equilibrium interaction analyses, we also introduce other MST-based applications: By adjusting experimental conditions, MST can be used to follow the kinetics of enzyme-substrate reactions, and it can also be used to precisely detect multi-step protein unfolding processes. Thus, MST is not limited to molecular interaction analyses, but constitutes a versatile tool to dissect a plethora of biomolecular properties.

Competing financial interests

MJW, HMR, TA, RW and DB are employees of NanoTemper Technologies GmbH. PB and SD are CEOs of NanoTemper Technologies GmbH.

Acknowledgements

We thank Manuela Gerhofer and Michael Pietschner for technical assistance. We thank Dr. Ute Curth, Dr. Ahmed Besheer, Prof. Dr. Gideon Schreiber and Prof. Dr. George Iliakis for generously providing reagents. This work was supported by the Bavarian Research Foundation (AZ-992-11), enzyme kinetic experiments were enabled by funds from ZIM (Zentrales Innovationsprogramm für den Mittelstand; EP110843).

Appendix A. Methods

Fig. 2A: Instrument and settings: Monolith® NT.115^{Pico}; MST power = 15%; LED power = 40%.

5′-Cy5-labeled template and complementary strands were purchased from Metabion (Martinsreid, Germany). DNA-oligonucleotide sequences are shown in Fig. 3A (Template and perfect match). Measurements were carried out in DNA-buffer (25 mM HEPES pH 7.4, 100 mM NaCl, 0.05% tween 20) and standard capillaries. Photobleaching was suppressed by removing molecular oxygen from the reaction mixture. This was achieved by using the NanoTemper Anti-Photobleaching kit (NanoTemper technologies, Munich, Germany), which contains a multi-component enzyme-substrate oxygen-scavenger system. Error bars = s.d. from three independent experiments.

Fig. 2B: Instrument and settings: Monolith® NT.115^{Pico}; MST power = 40%; LED power = 100%.

EcoSSB was a kind gift from Dr. Ute Curth and purified as described previously [16]. 5′-Cy5-labeled oligo(dT)$_{70}$ was obtained from Axolabs (Kulmbach, Germany). Measurements were carried out in SSB-buffer (20 mM HEPES pH 7.4, 300 mM NaCl, 0.05% tween 20) and standard capillaries. Photobleaching was suppressed using the NanoTemper Anti-Photobleaching kit. All pre-dilutions and dilution series were pipetted in low-binding tubes to prevent sample loss on tube walls. Error bars = s.d. from three independent experiments.

Fig. 2C: Instrument and settings: Monolith® NT.115^{Pico}; MST power = 40%; LED power = 80%.

IL-RI (R&D systems, Minneapolis, MN) was labeled on lysine residues with NT647 using the NanoTemper labeling kit (NanoTemper technologies, Munich, Germany). Measurements were carried out in MST-buffer (50 mM TrisHCl pH 7.8, 150 mM NaCl, 10 mM $MgCl_2$, 0.05% tween 20) and standard capillaries. Photobleaching was suppressed using the NanoTemper Anti-Photobleaching kit. Anakinra protein was a kind gift from Dr. Ahmed Besheer. Error bars = s.d. from three independent experiments.

Fig. 3A–D: Instrument and settings: Monolith® NT.115^{Pico}; MST power = 40%; LED power = 100%.

Measurements were carried out in SSB-buffer (20 mM HEPES pH 7.4, 300 mM NaCl, 0.05% tween 20) and standard capillaries. Cy5-labeled oligo(dT)$_{35}$ was obtained from Metabion (Martinsreid, Germany). Photobleaching was suppressed using the NanoTemper Anti-Photobleaching kit. All pre-dilutions and dilution series were pipetted in low-binding tubes to prevent sample loss on tube walls. Error bars = s.d. from three independent experiments.

Fig. 4C: Instrument and settings: Monolith® NT.115^{Pico}; MST power = 15%; LED power = 90%.

All DNA constructs were purchased from Metabion (Martinsreid, Germany). Measurements were carried out in DNA-buffer (25 mM HEPES pH 7.4, 100 mM NaCl, 0.05% tween 20) supplemented with 5 mM EDTA and standard capillaries. Photobleaching was suppressed using the NanoTemper Anti-Photobleaching kit. Binding curves were obtained over a temperature range from 25 °C to 45 °C at 1 °C increments regulated by the internal temperature control of the Monolith NT.115^{Pico} device. The concentration of the 5′-Cy5-labeled DNA 20-mer was kept constant at 1 nM and its perfect match or one of two mismatches were diluted in a range from 1600 nM down to 0.05 nM, respectively. For each temperature, MST measurements were started 120 s after reaching the desired temperature. K_d-values were calculated for each temperature by fitting the T-Jump signal, and plotted as $\ln(1/K_d)$ vs. $1/T$ (K) in an van't Hoff plot. ΔH° was obtained from the slope m of the linear fit as

$$m = \frac{-H^\circ}{R} \tag{3}$$

Under the assumption that ΔH° is constant in the relatively small linear range of the van't Hoff plot ΔS° was directly derived from the plot as

$$y(0) = \frac{\Delta S^\circ}{R} \quad (4)$$

The universal gas constant R was converted from SI units to [cal/mol *K].

Fig. 5A: Instrument and settings: Monolith® NT.LabelFree; MST power = 40%; LED power = 20%.

Carbonic anhydrase isozyme II from bovine erythrocytes was purchased from Sigma–Aldrich (St. Louis, MO). Measurements were carried out in 10 mM phosphate buffer (pH 8.0) and NT.LabelFree Standard treated capillaries. Samples containing 1 μM BCAII and increasing GdmCl concentrations were incubated for at least 4 h to reach equilibrium unfolding prior to experiments.

Fig. 5D: Instrument and settings: Monolith® NT.LabelFree; MST power = 10%; LED power = 20%. NT.LabelFree Standard Treated capillaries

Concanavalin A from *Canavalia ensiformis* (Jack bean) Type V was purchased from Sigma–Aldrich and used without further purification. Measurements were carried out in PBS (pH 7.2) and NT.LabelFree Standard treated capillaries. Samples containing 2 μM ConA and increasing concentrations of GdmCl were incubated for at least 5 h to reach equilibrium unfolding.

Fig. 6: DNase I was purchased from New England Biolabs (Ipswich, MA). The real time measurement was performed at 50% LED (blue channel) and 20% MST power, Laser-On time was 1 s, Laser-Off time 1 s. The quenching measurement was performed at 50 % LED (blue channel) and 20% MST power, Laser-On time was 30 s, Laser-Off time 5 s. For both the direct and the quenching approach, first-order kinetics were fitted using

$$[A] = [A]_0(1 - e^{t/\tau}) \quad (5)$$

Fig. 7: Instrument and settings: Monolith® NT.115; MST power = 80%; LED power = 80% (Fig. 6A); MST power = 40%; LED power = 80%. (Fig. 6B); MST power = 40%; LED power = 80% (Fig. 6C).

Binding of BLIP to NT647-TEM1: TEM1 was labeled on lysine residues with NT647 using the NanoTemper labeling kit. The concentration of labeled TEM1 protein was kept constant at a concentration of 5 nM. The unlabeled binding partner was titrated in 1:1 dilutions. The highest concentration of BLIP was 500 nM. Measurements were carried out in MST buffer. For measurements, samples were filled into standard treated capillaries.

Binding of Ypet-BLIP to mCherry-TEM1: The concentration of Ypet-BLIP protein was kept constant at 10 nM. The binding partner (mCherry-TEM1) was titrated in 1:1 dilutions. The highest concentration of TEM1-mCherry was 2500 nM. Samples were diluted in MST buffer. For measurements, samples were filled into standard treated capillaries.

Binding of Ypet-BLIP to mCherry-TEM1 in eukaryotic cell lysate:

Preparation of cell lysate: 2×10^7 293T cells were lysed using 1000 μl of Lysis-buffer (10% Glycerol, 0.1% NP-40, Protease Inhibitors). The cell lysate was centrifuged at 15,000 rpm for 5 min in order to remove large aggregates and cell debris.

Sample preparation: TEM1 was titrated in 1:1 dilutions (in cell lysate). Then Ypet-BLIP was added into 200 μl of 293T cell lysate to a final concentration of 10 nM. 10 μl of Ypet-BLIP-containing cell lysate was mixed with 10 μl cell lysate containing mCherry-TEM1 dilutions. For measurements, samples were filled into standard treated capillaries.

References

[1] D. Adams, P. Lozeron, C. Lacroix, Curr. Opin. Neurol. 25 (2012) 564–572.
[2] S. Albeck, G. Schreiber, Biochemistry 38 (1999) 11–21.
[3] B. Alberts, Nature 421 (2003) 431–435.
[4] C.G. Alexander, M.C. Jurgens, D.A. Shepherd, S.M. Freund, A.E. Ashcroft, N. Ferguson, Proc. Natl. Acad. Sci. USA 110 (2013) E2782–E2791.
[5] N. Arbel, D. Ben-Hail, V. Shoshan-Barmatz, J. Biol. Chem. 287 (2012) 23152–23161.
[6] P. Baaske, C.J. Wienken, P. Reineck, S. Duhr, D. Braun, Angew. Chem. Int. Ed. Engl. 49 (2010) 2238–2241.
[7] P. Baaske, C.J. Wienken, P. Reineck, S. Duhr, D. Braun, Angew. Chem. 122 (2010) 2286–2290.
[8] R. Baron, J.A. McCammon, Annu. Rev. Phys. Chem. 64 (2013) 151–175.
[9] W. Bujalowski, T.M. Lohman, J. Mol. Biol. 207 (1989) 249–268.
[10] W. Bujalowski, T.M. Lohman, J. Mol. Biol. 207 (1989) 269–288.
[11] N.A. Bushmarina, I.M. Kuznetsova, A.G. Biktashev, K.K. Turoverov, V.N. Uversky, Chembiochem: Eur. J. Chem. Biol. 2 (2001) 813–821.
[12] J.B. Chaires, Annu. Rev. Biophys. 37 (2008) 135–151.
[13] A. Chatterjee, D.K. Mandal, Biochim. Biophys. Acta 1648 (2003) 174–183.
[14] C. Chen, A. Constantinou, M. Deonarain, Expert Opin. Drug Delivery 8 (2011) 1221–1236.
[15] E.H. Choy, A.F. Kavanaugh, S.A. Jones, Nat. Rev. Rheumatol. 9 (2013) 154–163.
[16] U. Curth, C. Urbanke, J. Greipel, H. Gerberding, V. Tiranti, M. Zeviani, Eur. J. Biochem./FEBS 221 (1994) 435–443.
[17] C.A. Dinarello, Int. Rev. Immunol. 16 (1998) 457–499.
[18] M. Doetsch, S. Stampfl, B. Fürtig, M. Beich-Frandsen, K. Saxena, M. Lybecker, R. Schroeder, Nucleic Acids Res. (2012).
[19] S. Duhr, D. Braun, Phys. Rev. Lett. (2006) 96.
[20] S. Duhr, D. Braun, Phys. Rev. Lett. 96 (2006) 168301.
[21] S. Duhr, D. Braun, Proc. Natl. Acad. Sci. USA 103 (2006) 19678–19682.
[22] A.E. Eriksson, T.A. Jones, A. Liljas, Proteins 4 (1988) 274–282.
[23] M. Filarsky, Application Note NT005 (2012).
[24] E.C. Gaffarogullari, A. Krause, J. Balbo, D.P. Herten, A. Jaschke, RNA Biol. 10 (2013) 1815–1821.
[25] C.D. Geddes, Rev. Fluoresc., vol. XII, Springer, New York, 2011.
[26] T. Ha, P. Tinnefeld, Annu. Rev. Phys. Chem. 63 (2012) 595–617.
[27] F. Immekus, L.J. Barandun, M. Betz, F. Debaene, S. Petiot, S. Sanglier-Cianferani, K. Reuter, F. Diederich, G. Klebe, ACS Chem. Biol. (2013).
[28] M. Jerabek-Willemsen, C.J. Wienken, D. Braun, P. Baaske, S. Duhr, Assay Drug Develop. Technol. 9 (2011) 342–353.
[29] T. Keren-Kaplan, I. Attali, M. Estrin, L.S. Kuo, E. Farkash, M. Jerabek-Willemsen, N. Blutraich, S. Artzi, A. Peri, E.O. Freed, H.J. Wolfson, G. Prag, EMBO J. 32 (2013) 538–551.
[30] M. Kunitz, J. General Physiol. 33 (1950) 349–362.
[31] Z. Liao, R.S. Grimshaw, D.L. Rosenstreich, J. Exp. Med. 159 (1984) 126–136.
[32] Z. Liao, A. Haimovitz, Y. Chen, J. Chan, D.L. Rosenstreich, J. Immunol. 134 (1985) 3882–3886.
[33] C.C. Lin, F.A. Melo, R. Ghosh, K.M. Suen, L.J. Stagg, J. Kirkpatrick, S.T. Arold, Z. Ahmed, J.E. Ladbury, Cell 149 (2012) 1514–1524.
[34] C. Ludwig, Diffusion zwischen ungleich erwärmten Orten gleich zusammengesetzter Lösungen, Sitzungber Bayer Akad Wiss Wien Math-Naturwiss Kl, vol. 20, 1856.
[35] J. Luo, J. Zhou, W. Zou, P. Shen, J. Protein Chem. 18 (1999) 709–719.
[36] S. Maiti, U. Haupts, W.W. Webb, Proc. Natl. Acad. Sci. USA 94 (1997) 11753–11757.
[37] D. Martin, A. Charpilienne, A. Parent, A. Boussac, B. D'Autreaux, J. Poupon, D. Poncet, FASEB J.: Off. Publ. Fed. Am. Soc. Exp. Biol. 27 (2013) 1074–1083.
[38] A. Masi, R. Cicchi, A. Carloni, F.S. Pavone, A. Arcangeli, Adv. Exp. Med. Biol. 674 (2010) 33–42.
[39] E. Masini, F. Carta, A. Scozzafava, C.T. Supuran, Expert Opin. Therap. Patents 23 (2013) 705–716.
[40] T. Matsumoto, Y. Morimoto, N. Shibata, T. Kinebuchi, N. Shimamoto, T. Tsukihara, N. Yasuoka, J. Biochem. 127 (2000) 329–335.
[41] I. Mellman, G. Coukos, G. Dranoff, Nature 480 (2011) 480–489.
[42] J.J. O'Shea, A. Laurence, I.B. McInnes, Nat. Rev. Rheumatol. 9 (2013) 173–182.
[43] R. Owczarzy, A.V. Tataurov, Y. Wu, J.A. Manthey, K.A. McQuisten, H.G. Almabrazi, K.F. Pedersen, Y. Lin, J. Garretson, N.O. McEntaggart, C.A. Sailor, R.B. Dawson, A.S. Peek, Nucleic Acids Res. 36 (2008) W163–W169.
[44] S. Patnaik, W. Zheng, J.H. Choi, O. Motabar, N. Southall, W. Westbroek, W.A. Lea, A. Velayati, E. Goldin, E. Sidransky, W. Leister, J.J. Marugan, J. Med. Chem. 55 (2012) 5734–5748.
[45] T.H. Pham, J. Minderjahn, C. Schmidl, H. Hoffmeister, S. Schmidhofer, W. Chen, G. Langst, C. Benner, M. Rehli, Nucleic Acids Res. (2013).
[46] Y. Phillip, G. Schreiber, FEBS Lett. 587 (2013) 1046–1052.
[47] V.I. Razinkov, M.J. Treuheit, G.W. Becker, Curr. Drug Discov. Technol. 10 (2013) 59–70.
[48] C. Richter-Landsberg, O. Goldbaum, Cell. Mol. Life Sci.: CMLS 60 (2003) 337–349.
[49] N.A. Rodionova, G.V. Semisotnov, V.P. Kutyshenko, V.N. Uverskii, I.A. Bolotina, Molekuliarnaia Biologiia 23 (1989) 683–692.
[50] C. Rueckert, C.A. Guzman, PLoS Pathogens 8 (2012) e1003001.
[51] V.L. Schramm, Annu. Rev. Biochem. 80 (2011) 703–732.
[52] H. Schreuder, C. Tardif, S. Trump-Kallmeyer, A. Soffientini, E. Sarubbi, A. Akeson, T. Bowlin, S. Yanofsky, R.W. Barrett, Nature 386 (1997) 194–200.
[53] T. Schubert, M.C. Pusch, S. Diermeier, V. Benes, E. Kremmer, A. Imhof, G. Langst, Mol. Cell 48 (2012) 434–444.
[54] S.A. Seidel, P.M. Dijkman, W.A. Lea, G. van den Bogaart, M. Jerabek-Willemsen, A. Lazic, J.S. Joseph, P. Srinivasan, P. Baaske, A. Simeonov, I. Katritch, F.A. Melo,

J.E. Ladbury, G. Schreiber, A. Watts, D. Braun, S. Duhr, Methods 59 (2013) 301–315.
[55] S.A. Seidel, C.J. Wienken, S. Geissler, M. Jerabek-Willemsen, S. Duhr, A. Reiter, D. Trauner, D. Braun, P. Baaske, Angew. Chem. Int. Ed. Engl. 51 (2012) 10656–10659.
[56] G.V. Semisotnov, V.P. Kutyshenko, O.B. Ptitsyn, Molekuliarnaia Biologiia 23 (1989) 808–815.
[57] G.V. Semisotnov, N.A. Rodionova, O.I. Razgulyaev, V.N. Uversky, A.F. Gripas, R.I. Gilmanshin, Biopolymers 31 (1991) 119–128.
[58] M.F. Shamji, H. Betre, V.B. Kraus, J. Chen, A. Chilkoti, R. Pichika, K. Masuda, L.A. Setton, Arthritis Rheumatism 56 (2007) 3650–3661.
[59] X. Shang, F. Marchioni, C.R. Evelyn, N. Sipes, X. Zhou, W. Seibel, M. Wortman, Y. Zheng, Proc. Natl. Acad. Sci. USA 110 (2013) 3155–3160.
[60] N. Sharon, Cell. Mol. Life Sci.: CMLS 62 (2005) 1057–1062.
[61] N. Sharon, Biochem. Soc. Trans. 36 (2008) 1457–1460.
[62] K. Sigmundsson, G. Masson, R. Rice, N. Beauchemin, B. Obrink, Biochemistry 41 (2002) 8263–8276.
[63] T. Strauß, R.M.P. van Poecke, A. Strauß, P. Römer, G.V. Minsavage, S. Singh, C. Wolf, A. Strauß, S. Kim, H.-A. Lee, S.-I. Yeom, M. Parniske, R.E. Stall, J.B. Jones, D. Choi, M. Prins, T. Lahaye, Proc. Natl. Acad. Sci. 109 (2012) 19480–19485.
[64] V.N. Uverskii, O.B. Ptitsyn, Molekuliarnaia Biologiia 30 (1996) 1124–1134.
[65] M.A. Uzarska, R. Dutkiewicz, S.A. Freibert, R. Lill, U. Muhlenhoff, Mol. Biol. Cell (2013).
[66] G. van den Bogaart, K. Meyenberg, U. Diederichsen, R. Jahn, J. Biol. Chem. 287 (2012) 16447–16453.
[67] G. van den Bogaart, S. Thutupalli, J.H. Risselada, K. Meyenberg, M. Holt, D. Riedel, U. Diederichsen, S. Herminghaus, H. Grubmuller, R. Jahn, Nat. Struct. Mol. Biol. 18 (2011) 805–812.
[68] S. Vanecko, M. Laskowski Sr., J. Biol. Chem. 236 (1961) 1135–1140.
[69] S. Vanecko, M. Laskowski Sr., J. Biol. Chem. 236 (1961) 3312–3316.
[70] C.J. Wienken, P. Baaske, S. Duhr, D. Braun, Nucleic Acids Res. 39 (2011) e52.
[71] C.J. Wienken, P. Baaske, U. Rothbauer, D. Braun, S. Duhr, Nat. Commun. 1 (2010) 100.
[72] S.M. Wilson, B.S. Schmutzler, J.M. Brittain, E.T. Dustrude, M.S. Ripsch, J.J. Pellman, T.S. Yeum, J.H. Hurley, C.M. Hingtgen, F.A. White, R. Khanna, J. Biol. Chem. 287 (2012) 35065–35077.
[73] X. Xiong, P.J. Coombs, S.R. Martin, J. Liu, H. Xiao, J.W. McCauley, K. Locher, P.A. Walker, P.J. Collins, Y. Kawaoka, J.J. Skehel, S.J. Gamblin, Nature 497 (2013) 392–396.
[74] A. Yazgan, R.W. Henkens, Biochemistry 11 (1972) 1314–1318.
[75] H.X. Zhou, G. Rivas, A.P. Minton, Annu. Rev. Biophys. 37 (2008) 375–397.
[76] K. Zillner, M. Filarsky, K. Rachow, M. Weinberger, G. Langst, A. Nemeth, Nucleic Acids Res. 41 (2013) 5251–5262.
[77] K. Zillner, M. Jerabek-Willemsen, S. Duhr, D. Braun, G. Langst, P. Baaske, Meth. Mol. Biol. 815 (2012) 241–252.